



HAL
open science

Picosecond laser beam nanostructuring of GDC thin films: exchange surface enhancement by LIPSS

Wael Karim, Agnès Petit, Hervé Rabat, Malek Tabbal, Anne-Lise Thomann, Nadjib Semmar

► To cite this version:

Wael Karim, Agnès Petit, Hervé Rabat, Malek Tabbal, Anne-Lise Thomann, et al.. Picosecond laser beam nanostructuring of GDC thin films: exchange surface enhancement by LIPSS. Applied physics. A, Materials science & processing, 2022, 128 (8), pp.731. 10.1007/s00339-022-05866-6 . hal-04056136v1

HAL Id: hal-04056136

<https://cnrs.hal.science/hal-04056136v1>

Submitted on 21 Nov 2022 (v1), last revised 4 Dec 2023 (v2)

HAL is a multi-disciplinary open access archive for the deposit and dissemination of scientific research documents, whether they are published or not. The documents may come from teaching and research institutions in France or abroad, or from public or private research centers.

L'archive ouverte pluridisciplinaire **HAL**, est destinée au dépôt et à la diffusion de documents scientifiques de niveau recherche, publiés ou non, émanant des établissements d'enseignement et de recherche français ou étrangers, des laboratoires publics ou privés.

Picosecond laser beam nanostructuring of GDC thin films: exchange surface enhancement by LIPSS

Wael Karim¹, Agnès Petit¹, Hervé Rabat¹, Malek Tabbal², Anne-Lise Thomann¹ and Nadjib Semmar^{1*}

1. GREMI-UMR 7344-CNRS-University of Orleans, 14 Rue d'Issoudun, BP6744, 45067 Orléans Cedex, France

2. Department of Physics, American University of Beirut, Beirut, Lebanon 1107 2020.

*Corresponding author: Nadjib.semmar@univ-orleans.fr

Abstract

In ceramic electrochemical cells, gadolinium-doped ceria (GDC) thin film is deposited between the electrolyte (yttria-stabilized zirconia, YSZ) and the upper electrode in order to improve the aging resistance. Increasing the interface surface area is expected to be beneficial to the cell performance. This work investigates the formation of LIPSS (Laser induced periodic surface structures) on the surface of a 600 nm GDC thin films grown by magnetron sputtering on screen-printed YSZ. A picosecond Nd: YAG laser operating at its third harmonic ($\lambda=355$ nm, 40 ps, 10Hz) was used to structure the surface of the GDC/YSZ layer after deposition, thanks to static and scanning irradiation modes. The different structures formed on the film surface following laser irradiation, mainly quasi-periodic LIPSS, were investigated by Scanning Electron Microscopy (SEM) and Atomic Force Microscopy (AFM). Parallel and perpendicular LIPSS were simultaneously formed with periods varying from 220 to 300 nm, as a function of the beam fluence ranging from 30 to 160 mJ/cm², and within a spot size of ~500 μ m in the static mode. The coexistence of the two orientations disappeared at a higher number of shots ($N > 20$), where only parallel structures were formed. Increasing the number of shots up to $N > 50$ led to a progressive ablation of the film followed by the start of a process of YSZ substrate nano-structuring. The formation of parallel LIPSS is mainly attributed to the thermochemical process that occurs on the GDC/YSZ film in the center of the irradiated zone corresponding to the highest local fluence. The same LIPSS orientations were also found in the scanning mode by varying the laser fluence and the scanning stage parameters. For the latter mode, the effect of laser irradiation on the elemental composition of the films was investigated by Energy Dispersive X-Ray spectroscopy (EDX) and Rutherford Back-Scattering (RBS) to check the film chemical stability under the process of soft ablation by accumulation effect. Finally, the surface area enhancement by LIPSS formation was estimated thanks to Atomic Force

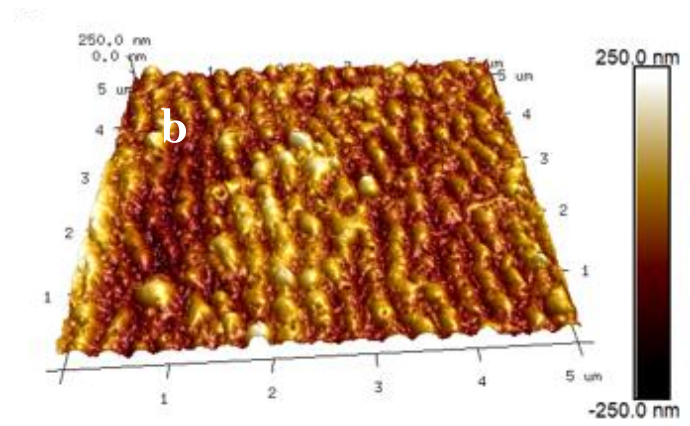
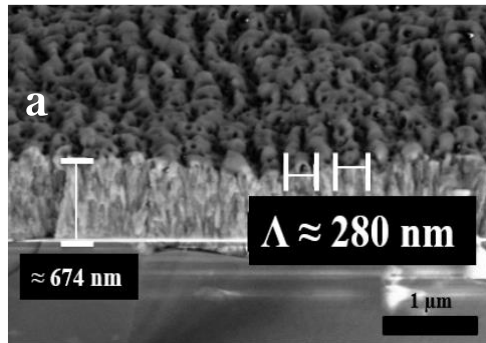
Microscopy (AFM) and using a geometrical enhancement coefficient that returned ‘theoretical’ maximum values of 57% and 78 % for 1D (regular LIPSS) and 2D periodic structures respectively, and 41% for the experimental case.

Keywords: Picosecond laser beam; oxide thin film; GDC magnetron sputtered film; multi-pulse irradiation; LIPSS.

Highlights

- LIPSS formation was achieved on gadolinium doped ceria (GDC) thin films under static and scanning beam modes.
- Laser texturing was successfully performed using a pico-second Nd:YAG laser with a beam spot diameter close to 500 μm .
- Experimental conditions for obtaining parallel and perpendicular LIPSS and the occurrence of film ablation were determined.
- Results are explained through the existence of soft ablation by accumulation effects and thermochemical process at higher local fluence.
- The surface enhancement due to laser texturing is estimated to be over 30% using AFM and a geometrical model.

Graphical abstract



Introduction

The interaction between ultrashort laser beam pulses and solid-state materials can result in the formation of surface micro/nanostructures that are commonly referred to as Laser Induced Periodic Surface Structures (LIPSS). The size, shape and distribution of these structures show a complex dependence on the experimental conditions (such as laser energy, wavelength, repetition rate, scanning speed) as well as the type of material irradiated (metals, semiconductor, dielectric, ceramic or polymer) [1-7]. An understanding of LIPSS formation and a good control of their characteristics is crucial since their presence significantly modifies the surface properties of the material, which can thus be “tuned” for a specific application. LIPSS formation has indeed been shown to improve the mechanical and wetting properties of surfaces in addition to several other applications in a wide array of technological fields [8-13]. Building on the potential of laser texturing of the surface of bulk material, LIPSS formation on thin films has recently generated great interest both from the fundamental and technological aspects [14-17]. Compared to the case of bulk materials, the physico-chemical processes occurring during the laser irradiation of a thin film are markedly altered, typically with the observation of, for example, a lowering of the material’s ablation threshold, the occurrence of cavitation as well as thermomechanical fragmentation [18-21]. From a technological viewpoint, LIPSS formation on thin films could provide an attractive one-step approach to material micro/nano-structuring for functional coatings and advanced devices.

This work deals specifically with the investigation of LIPSS formation on the surface of gadolinium-doped ceria (GDC) thin films grown by magnetron sputtering on screen-printed yttria-stabilized zirconia (YSZ). GDC and YSZ are complex oxides that are employed in solid ceramic cell technology [22-24] due to their high ionic conductivity. A thin layer of GDC sandwiched between the electrolyte and the upper electrode ($\text{La}_{1-x}\text{Sr}_x\text{Co}_{1-y}\text{Fe}_y\text{O}_{3-\delta}$) can act as a diffusion barrier and has been found to improve the lifetime of cells dedicated to the production of hydrogen by high temperature electrolysis. With the aim of improving the efficiency of the cell, one interesting approach would be to increase the surface area where the electrochemical reactions take place, namely the actual area of the interface between the electrolyte (YSZ) and the upper electrode. In the present study, a picosecond Nd: YAG laser operating at the third harmonic ($\lambda=355$ nm) was used to structure the surface of the GDC layer after deposition, both in static and scanning modes. The different structures formed on the film surface following laser irradiation were investigated by Scanning Electron Microscopy (SEM) and Atomic Force Microscopy (AFM) **with tapping mode**. A mapping of the different surface morphologies as a function of irradiation conditions was thus achieved for the static mode. The

effect of laser irradiation on the elemental composition of the films was also investigated by Energy Dispersive X-Ray spectroscopy (EDX) and Rutherford Back-Scattering (RBS). Lastly, surface area enhancement by LIPSS formation is discussed using a simple model based on the morphological arrangement of the induced nanostructures.

Experimental

Gadolinium-doped ceria (GDC) thin films, with thicknesses of around 600 nm were deposited by direct current magnetron sputtering of 4-inch diameter metallic $Ce_{1-x}Gd_x$ targets ($x=0.2$) on screen-printed Yttrium-Stabilized Zirconium (YSZ) substrates (having thicknesses $\geq 1 \mu\text{m}$) provided by the CEA Le Ripault. All deposition runs were performed at a pressure of 1 Pa with 20 sccm of Ar as a sputtering gas and 2 sccm of O_2 as a reactive gas. The substrates were not heated during growth. The as-deposited films were subsequently annealed in air at 500 °C, a process that resulted in highly crystalline and stoichiometric layers ($Ce_{1-x}Gd_xO_2$). More details about growth conditions and film properties were presented elsewhere by Mickan et al. [25].

The laser irradiation experiments were achieved using a picosecond Nd: YAG laser operating at its third harmonic ($\lambda = 355 \text{ nm}$) with a pulse duration of 40 ps and 10 Hz repetition rate. The corresponding irradiation process is shown on Fig.1. The energy/pulse is modulated using a set of optical filters (UGC from Thorlabs), and the Gaussian beam of the laser is then focused on the surface of the sample using a quartz lens with a focal distance of 75 mm. For the present study, the laser fluence of the incident beam (F) was varied from 30 to 125 mJ/cm^2 . Samples were irradiated in static mode (by accumulation of successive single spots) and in scanning mode (large-area irradiation achieved by S-scanning) in air under atmospheric conditions. In static mode, the total number of shots (N) irradiating the same area of the sample is accurately controlled via an automated opto-mechanical shutter. Under scanning mode conditions, the sample is mounted on a motorized X, Y computer-controlled scanning stage. In order to irradiate the whole surface of the films, an S-shaped scanning pattern is achieved via a LabVIEW interface. Thanks to an automated scanner system (Scanner Newport-Conex CC with accessible speed ranging from 0.01 to 5 mm/s in the X, Y directions, with a translation path $\Delta Y = 100 \mu\text{m}$), the sample is moved along the x-axis at a speed V_x and displaced by a distance ΔY (perpendicular to the x-axis) at the end of the motion. The values of V_x used in the work were varied from 50 $\mu\text{m}/\text{s}$ up to 5 mm/s.

The surface morphology of the thin films before and after laser irradiation was observed using a Carl Zeiss SMT SUPRA 40 Field Emission Gun SEM, and their chemical composition determined using EDX. LIPSS amplitude and periodicity were determined through surface imaging using a Bruker AFM. Finally, RBS analysis was performed using α particles of 2 MeV extracted from a Pelletron accelerator in the CEMHTI laboratory (CNRS-Orléans, France).

Results

Irradiation under static mode

Figure 2 shows a typical SEM image of the surface of a GDC film irradiated under static mode with 10 laser pulses at a fluence of 125 mJ/cm^2 and a large spot size close to $500 \text{ }\mu\text{m}$. Careful observation enables several different regions on the image to be delimited, corresponding to the insets within the figure. First, the non-irradiated surface of the GDC films exhibits the grain boundaries of the polycrystalline YSZ layer (micron-sized grains) decorated by the GDC film [25]. The laser impact region, reasonably approximated to be circular with a diameter $W_0 \approx 500 \text{ }\mu\text{m}$, can be distinguished within which, two nearly circular concentric regions were imaged by SEM at higher resolution (see insets). The two different regions correspond to the formation of unexpected periodic patterns having different orientations with respect to the beam polarization. Quasi-regular LIPSS with orientation perpendicular to the laser beam (see bottom inset of the figure) are visible on the border of the irradiated zone. These LIPSS are formed at lower energy density (keeping in mind the beam Gaussian distribution) and are found to have a spatial period $\Lambda \sim 265 \pm 10 \text{ nm}$, lower than the laser wavelength ($\lambda=355 \text{ nm}$), and denoted as LSFL_\perp . In the center of the laser spot, which corresponds to the highest local fluence, unexpected LIPSS oriented parallel to the polarization of the laser beam with a spatial period of about $245 \pm 10 \text{ nm}$ are also observed and denoted as LSFL_\parallel , as indicated in the bottom inset of figure 2. The formation of two LIPSS patterns with different spatial periods and different directions was already observed in the case of HSFL and LSFL formation within the same spot zone [26] [27], on several metal and dielectric materials as well as on polymer thin films [28-30] but was rarely evidenced on a complex oxide substrate with such close spatial periods. Using a similar picosecond laser at the fourth harmonic (266 nm), Huynh et al. [16] found LSFL with a period of 260 nm on the surface of a Cu thin film. After increasing the number of shots to very high values, HSFL and LIPSS dots were formed. Considering another

metallic film but under scanning mode, Dostovalov et al. [31] found on the Cr surface, irradiated with a femtosecond laser ($\tau = 232$ fs; $\lambda = 1026$ nm; $f = 200$ kHz), LSFL-like structures ($\Lambda_{\text{LSFL}} = 696, 704, 816, \text{ and } 858$ nm) for a scanning speed $V = 1, 10, 50$ and 100 $\mu\text{m/s}$, respectively. In both studies, the LSFL obtained were in the range $(0.6 \text{ to } 0.9)\lambda$, parallel to the laser beam polarization, which is very similar to our unexpected case of LSFL $_{//}$ structures. On the contrary, Talbi et al. [17] managed to texture a thin layer of dielectric (titanium oxide $\text{TiO}_{1.2}$) and obtained LSFL structures perpendicular to the beam polarization with a period of 800 nm, using a femtosecond laser with a wavelength of 1030 nm and a pulse duration of 500 fs. As reported earlier in several theories debating on the LIPSS mechanism [12], [32-33], the formation of LIPSS parallel or perpendicular to the laser beam polarization is mainly related to the nature of the material surface (electronic, optical, thermal properties...) and the laser beam features (polarization, intensity, repetition rate...). Dostovalov et al. [34] studied the mechanism of LIPSS formation in Cr thin film material subject to oxidation. The oxidation level (depending on the film thickness) during the irradiation was found to induce a significant change in the optical properties as a consequence of the physico-chemical nature of the oxide film, and thus in the LIPSS orientation, parallel or perpendicular to the beam polarization. The particular ‘thermochemical’ conditions leading to oxidation during the irradiation of thin metal films were also investigated by Oktem et al. [35] on Ti thin films. The authors proposed a new paradigm through the ‘positive feedback’ approach for highly regular LIPSS formation. In such cases, the nanostructures formed were identified as thermochemical LIPSS (TLIPSS). To support this assumption (TLIPSS formation) for the LSFL $_{//}$ formed on GDC/YSZ in the center of the irradiated zone further chemical investigations are needed, for example by using XPS analysis (not shown in the present work) for an accurate estimation of the oxygen contribution. Moreover, it has been found in the literature that above 700°C , annealed GDC can lose part of its oxygen content. This leads to an increase in the non-stoichiometric coefficient δ ($\text{Ce}_{0.8}\text{Gd}_{0.2}\text{O}_{2-\delta}$), which can induce a lattice expansion, commonly referred to as "chemical expansion". This may originate from the growth of the cation radii during the reduction reactions taking place inside the CGO layers [36][37]. Thus, the Ce^{4+} ions incorporated in CGO transform into Ce^{3+} ions, which can locally generate a mixed ionic electronic conductivity (MIEC) [38]. As previously mentioned, due to the Gaussian beam distribution, the local fluence is highest at the center of the laser spot, so that the temperature can locally exceed the value (considering also the reaction time over this temperature threshold) at which GDC acquires MIEC properties. This could induce a *transient* ‘metallic’ behavior followed by intense back-oxidation that probably induces the formation of LSFL $_{//}$.

Further inspection of the LIPSS formation at different laser fluences led to finding a dependence of the LIPSS spatial period on laser fluence as shown in Figure 3 for both types of LIPSS, LSFL_{//} and LSFL_⊥. The figure shows that the spatial periods for each type move closer to each other as the laser fluence is increased from 60 mJ to 125 mJ/cm², increasing (decreasing) from 220 (300) to 245 (265) nm, respectively. The values of the spatial periods thus range from 0.6λ to 0.85λ, and these are known to depend on the refractive index n of the irradiated material. This also tends to confirm the correlation between the oxidation stage, the chemical expansion and thus the changes in optical properties. Thanks to the results reported in Dostovalov et al. [34], the diminution of the LSFL_⊥ period versus fluence can be related to the ‘soft’ ablation process and the reduction in film thickness, while the slight increase in the LSFL_{//} period is attributed to chemical expansion followed by more intense re-oxidation. Note that in such a complex situation, intermediate 2D-like structures are localized in the transition zone between the center and rim of the irradiated zone as previously shown on fig. 2.

To investigate the (F, N) domain of LIPSS formation and their singular orientation, the fluence and the number of shots were regularly increased up to complete ablation of the GDC film. Figure 4 shows SEM images of the surface of the GDC/YSZ samples irradiated at laser fluences between 40 and 125 mJ/cm², and numbers of shots ranging from 10 to 70. Different surface morphologies are observed depending on the laser fluence and number of laser pulses. At the lowest fluence, namely 40 mJ/cm², LSFL_⊥ are observed at N=10 and N=40, Fig 4.a and 4.b, respectively. In the latter case however, the LIPSS do not appear to be regularly formed. Increasing the number of pulses to 70 leads to the loss of the LIPSS patterns by ablation and re-deposition of the GDC films (Fig. 4.c). On increasing the laser fluence to 105 and 125 mJ/cm², both parallel and perpendicular LIPSS are still formed, as shown in Fig.4.d and Fig.4.g where the reported SEM images were taken at different places of the irradiated area (separated by the red line in the figure). As shown before, the LSFL_⊥ were found near the borders of the laser spot, and the LSFL_{//} appear in the center. Static irradiation with 30 pulses at 105 mJ/cm² leads to the loss of the LIPSS pattern (Fig.4.e) and this becomes more pronounced after 50 pulses (Fig.4.f) where the crystalline grain boundaries of the underlying YSZ become exposed. It is noteworthy that the loss of the LIPSS pattern takes place at a smaller number of pulses with increasing laser fluence, i.e. at 30 laser pulses at 105 mJ/cm² instead of 70 for a laser fluence of 40 mJ/cm². At even higher fluence, 125 mJ/cm², and after 30 and 50 laser pulses, the

GDC film appears to be completely ablated and is accompanied by patterning of the YSZ into square shapes.

The chemical composition of the surfaces after laser irradiation was investigated using EDX analysis. To that end, the representative signals for films irradiated at different laser fluences and number of laser pulses are reported in Fig.5, along with that of the untreated film. The insets included in the figure correspond to the SEM images shown in Fig. 4. On the EDX spectra of the untreated sample (Fig.5.a) and that of a film irradiated with 10 pulses at 40 mJ/cm² (Fig.5.b) exhibiting LIPSS, similar Ce and Gd signals are detected, whereas no signal emanating from the underlying YSZ substrate is evidenced. This confirms that the LIPSS patterns formed retain, within the accuracy limit of EDX, the same chemical composition as the starting material. With the loss of LIPSS formation for N = 70 at the same laser fluence (Fig.5.c), the EDX signals from the Ce and Gd become very low and in addition a broad peak corresponding to Y and Zr (the overlapping signals from these two elements is due to their close atomic masses, 89 and 91 u) is detected. This confirms the onset of ablation suggested from the SEM image for these irradiation conditions (Fig.4.c). The same trends are visible on Fig.5.d for a laser fluence of 150 mJ/cm² and a number of pulses of 40. This confirms that the square-shaped pattern seen in the inset of Fig.5.d can be attributed to laser surface structuring of the YSZ substrate (though some traces of the GDC film may remain). These patterns are quite similar to those obtained at 125 mJ/cm² for N = 30 and 50, Fig.4.h and i, and evidence the almost complete ablation of the GDC film.

Based on the parametric study presented above, a mapping of the laser induced surface modification of the GDC films grown on YSZ is suggested in Fig.6, as laser fluence and number of laser pulses are varied from 30 to 150 mJ/cm² and 1 to 70, respectively. The SEM and EDX observations allow us to delimit five distinguishable domains whose formation is dependent on the local energy dose.

In summary: LIPSS formation is not possible for $F < 40$ mJ/cm² (presented in gray). At higher fluence values (85 to 125 mJ/cm²), LSFL_{//} and LSFL_⊥ (in red) were generated but with $N < 20$.

Each phenomenon exists in a given area of the plot, i.e. over a given range of fluence and number of laser pulses. For instance, ablation occurs at a higher laser pulse number when the fluence is decreased. This is an indication that the ablation threshold is related to a parameter proportional to $F \cdot N$ (total deposited energy dose), which is the sign of an incubation phenomenon. The same behavior is observed for the formation of both kinds of LSFL. In Figure 7, we present a schematic that depicts the various energy dose thresholds for the formation of perpendicular and parallel LIPSS as well as the threshold for GDC full ablation that also corresponds to the starting point of YSZ structuring.

Irradiation under scanning mode

To estimate the enhancement of the exchange area on an extended treated surface of GDC film we performed laser irradiation on a wide surface area (minimum 4 X 4 mm²) by moving the sample holder in the X, Y directions as indicated on Fig. 1.

The starting point of our scanning strategy is based on the (F, N) mapping plot (fig.6) to reproduce on a large scale the LIPSS with the two main findings of the static mode: $F=125$ mJ/cm², $N < 20$ conditions corresponding to the co-existence of LSFL_{//} and LSFL_⊥, and $F = 85$ mJ/cm², $20 < N < 30$ conditions to lie in the pure LSFL_⊥ domain. Results for both operating conditions are plotted on figure 8 when the N becomes N_{eff} calculated from a standard formula that links the repetition rate f and the spot size d to the scanner speed V_x and the transverse path ΔY (i.e., $N_{eff} = (d \cdot f) / V_x \cdot (d / \Delta Y)$). As shown on the corresponding SEM images, while the first condition reproduces similar

regular structures as in the static mode, the second one ($F=125 \text{ mJ/cm}^2$, $N_{eff} = 10$) shows more complex patterns due to the superposition of parallel and perpendicular LSFL induced by the overlap of the successive irradiations. We also conducted the same EDX analyses as for the static mode with similar conclusions for the CGO film. However some redeposition is observed for the higher fluence ($F=125 \text{ mJ/cm}^2$), suggesting that a deeper investigation of the limit parameters is required to achieve full ablation of the film.

For this purpose, we investigated laser irradiation of the GDC films for $F = 40, 85, 125$ and 150 mJ/cm^2 under two (low) scanning speeds 0.2 and 0.4 mm/s ($N_{eff} = 125, 65.5$ respectively). SEM images of these laser irradiated surfaces are shown in Fig. 9. For $F = 40 \text{ mJ/cm}^2$, no LIPSS are detected for a scanning speed of 0.4 mm/s (Fig.9.a1) but some regular rippling indicating the onset of LIPSS formation is observed at 0.2 mm/s , (Fig.9.a2). Increasing the value of laser fluence to 85 mJ/cm^2 , LIPSS are formed even at the higher scanning speed of 0.4 mm/sec (Fig.9.b1) and appear somewhat similar to those obtained at 0.2 mm/sec (Fig.9.b2). This implies that the energy threshold to obtain LIPSS is reached even at the highest speed. A further increase of laser fluence up to 125 mJ/cm^2 still results in well-ordered LIPSS at $V = 0.4 \text{ mm/s}$ (Fig.9.c1). But at a lower scanning speed (0.2 mm/s), ablation of the thin layer of GDC takes place (Fig.9.c2). Finally, for the highest laser fluence used in this work, namely 150 mJ/cm^2 , GDC film ablation is observed at $V = 0.4 \text{ mm/s}$ (Fig.9.d1) and becomes nearly complete at $V = 0.2 \text{ mm/s}$ (Fig.9.d2). At such a speed and laser fluence, the grain boundaries of the YSZ substrate become exposed and the substrate itself becomes regularly patterned into square shaped structures, **probably due to surface cracking**, as observed for the highest laser fluence and number of pulses in the static irradiation case (Fig. 6.j). As indicated previously, during this ablation process we only reproduced the $LSFL_{\perp}$ before the full removal of the GDC thin film

Figure 10 shows two SEM images of the cross section of the GDC layer. The first one is the untreated layer and the other one a layer textured by laser scanning at a fluence of 85 mJ/cm^2 and a velocity $V = 0.4 \text{ mm/s}$. First of all it is clearly visible that the GDC film in-depth microstructure changes greatly. The well-aligned columns of about 100 nm width are not present any more, and have been replaced by less regular patterns.

It can also be noticed that the thickness of the layer has decreased by about 100 nm, which confirms the partial ablation that occurs for this condition.

In addition, RBS measurements, illustrated in Figure 11, were performed on these two samples to confirm the thickness reduction after laser structuring. From simulation of the spectra, it can be deduced that there was a 17% decrease of the Ce and Gd atoms/cm² after laser treatment, while the proportions of YSZ and O remained unchanged. And finally, the shape of the spectra at the interface between GDC and YSZ layers indicates that the roughness of the layer increases, which is in good agreement with the SEM images of figure 10.

Estimation of the surface area increase by LIPSS

The surface modification due to the formation of nanostructures can be evaluated through some simple geometrical considerations. We estimated the surface enhancement due to LIPSS fabrication using the geometrical model detailed in the Appendix. From the set of equations (6* and 7*), the maximum theoretical enhancement coefficient (Σ) cannot exceed 57% in the case of regular 1D LIPSS and 78% in the case of 2D LIPSS (nanodots, nanobumps...). This maximum is only achieved in the case of contiguous LIPSS, i.e. the situation for $2r \approx \Lambda$, where r is here the specific radius of the nanostructure (assumed uniform), and Λ the spatial period. However, the major cases of LIPSS configurations correspond to the case $2r/\Lambda < 1$, and as reported in Table 1, the estimation of the enhancement coefficient Σ returns values in the range of 10 to 40%, which is far from the theoretical values. Considering the LIPSS sizes obtained on Fig. 12 (better resolution of the cross section and tilted SEM image), we performed the same estimation of the Σ coefficient in the case of GDC and compared this value to literature values, summarized in Table 1. On the other hand, thanks to the AFM mathematical toolbox, it was possible to estimate directly the GDC surface morphology changes before and after the beam irradiation in the conditions $F=85\text{mJ/cm}^2$ and $V = 0.4 \text{ mm/s}$. In this case, the difference between the irradiated film surface and the 'as deposited' one was estimated to be close to 40% (42 % in the case of a $5 \times 5 \mu\text{m}^2$ AFM scanned zone, and 39 % for the case $2 \times 2 \mu\text{m}^2$). Both values are relatively high compared to the literature cases, and in good agreement with the calculated Σ coefficient namely for the case of the nanosquared LIPSS (superposition of parallel and perpendicular LIPSS).

Conclusion

We demonstrated the feasibility of nanostructuring with quasi-periodic LIPSS GDC sputtered films deposited onto a screen-printed YSZ substrate using a UV picosecond laser beam with a low repetition rate. Static and scanning irradiation modes were investigated according to the fluence and number of pulses. In the static mode, two unexpected LSFL orientations were formed within the same irradiated area for F varying from 85 up to 125 mJ/cm² but only for a low number of accumulated pulses ($N < 20$). The formation of parallel LSFL is supported by the thermochemical oxidation origin and the transition to the MIEC state that occurs in the center of the irradiated zone for higher accumulated energy doses. With higher numbers of pulses, the GDC film is progressively ablated, resulting in the step-by-step removal of the film followed by the square-like patterning of the YSZ substrate. In the dynamic mode and for equivalent conditions $F = 85$ mJ/cm² and $N_{eff} = 25$, LSFL were formed on a large area (4X4 mm²) with a parallel orientation, whereas a more complex patterning was achieved at $F = 125$ mJ/cm², and $N_{eff} = 10$ attributed to the overlap and the superposition of parallel and perpendicular LSFL. The scanning limits leading to the progressive ablation of the GDC film were also investigated until the full removal of the film and the starting point of YSZ substrate patterning. Lastly, the enhancement of the exchange surface area estimated by a simple geometrical model and direct AFM measurements for the condition $F = 85$ mJ/cm² and $V = 0.4$ mm/s is estimated to be close to 33% for LSFL// and to 40% for the nanosquared LIPSS.

Acknowledgement

The authors would like to thank **Julien Vulliet** from the CEA Le Ripault for providing the screen-printed YSZ substrates, and the ‘Région Centre-Val-de-Loire’ for funding via the ‘ARD Lavoisier’ program.

Conflicts of Interest: The authors declare no conflict of interest.

References

- [1] A. Nakhoul *et al.*, « Self-Organization Regimes Induced by Ultrafast Laser on Surfaces in the Tens of Nanometer Scales », *Nanomaterials*, vol. 11, n° 4, Art. n° 4, Apr. 2021, DOI: 10.3390/nano11041020.
- [2] L. P. Rivera, D. Munoz-Martin, A. Chávez-Chávez, M. Morales, G. Gómez-Rosas, & C. Molpeceres, « Subwavelength LIPSS formation on SS304 by picosecond laser irradiation under water confinement », *Mater. Sci. Eng. B*, vol. 273, p. 115393, Nov. 2021, DOI: 10.1016/j.mseb.2021.115393.
- [3] J. Bonse, H. Sturm, D. Schmidt, & W. Kautek, « Chemical, morphological and accumulation phenomena in ultrashort-pulse laser ablation of TiN in air », *Appl. Phys. Mater. Sci. Process.*, vol. 71, n° 6, Art. n° 6, Dec. 2000, DOI: 10.1007/s003390000585.
- [4] A. Borowiec & H. K. Haugen, « Subwavelength ripple formation on the surfaces of compound semiconductors irradiated with femtosecond laser pulses », *Appl. Phys. Lett.*, vol. 82, n° 25, Art. n° 25, June 2003, DOI: 10.1063/1.1586457.
- [5] A. De Zanet, V. Casalegno, & M. Salvo, « Laser surface texturing of ceramics and ceramic composite materials – A review », *Ceram. Int.*, vol. 47, n° 6, Art. n° 6, Mar. 2021, DOI: 10.1016/j.ceramint.2020.11.146.
- [6] F. Costache, M. Henyk, & J. Reif, « Modification of dielectric surfaces with ultrashort laser pulses », *Appl. Surf. Sci.*, p. 6, 2002, DOI: 10.1016/S0169-4332(01)00675-4
- [7] Q. Li *et al.*, « Femtosecond laser-induced periodic surface structures on lithium niobate crystal benefiting from sample heating », *Photonics Res.*, vol. 6, n° 8, Art. n° 8, Aug. 2018, DOI: 10.1364/PRJ.6.000789.
- [8] E. Stratakis *et al.*, « Laser engineering of biomimetic surfaces », *Mater. Sci. Eng. R Rep.*, vol. 141, p. 100562, July 2020, DOI: 10.1016/j.mser.2020.100562.
- [9] J. Bonse, S. Hohm, S. V. Kirner, A. Rosenfeld, & J. Kruger, « Laser-Induced Periodic Surface Structures— A Scientific Evergreen », *IEEE J. Sel. Top. Quantum Electron.*, vol. 23, n° 3, Art. n° 3, May 2017, DOI: 10.1109/JSTQE.2016.2614183.
- [10] M. Ahn *et al.*, « Low damage electrical modification of 4H-SiC via ultrafast laser irradiation », *J. Appl. Phys.*, vol. 123, n° 14, p. 145106, Apr. 2018, DOI: 10.1063/1.5020445.
- [11] A. Y. Vorobyev & C. Guo, « Direct femtosecond laser surface nano/microstructuring and its applications », *Laser Photonics Rev.*, vol. 7, n° 3, Art. n° 3, May 2013, DOI: 10.1002/lpor.201200017.
- [12] J. Reif, O. Varlamova, S. Uhlig, S. Varlamov, & M. Bestehorn, « On the physics of self-organized nanostructure formation upon femtosecond laser ablation », *Appl. Phys. A*, vol. 117, n° 1, Art. n° 1, Oct. 2014, DOI: 10.1007/s00339-014-8339-x.
- [13] E. L. Gurevich & S. V. Gurevich, « Laser Induced Periodic Surface Structures induced by surface plasmons coupled via roughness », *Appl. Surf. Sci.*, vol. 302, p. 118-123, May 2014, DOI: 10.1016/j.apsusc.2013.10.141.
- [14] P. Liu, W. Wang, A. Pan, Y. Xiang, & D. Wang, « Periodic surface structures on the surface of indium tin oxide film obtained using picosecond laser », *Opt. Laser Technol.*, vol. 106, p. 259-264, Oct. 2018, DOI: 10.1016/j.optlastec.2018.04.019.

- [15] C. Deng *et al.*, « Photocatalytic performance of TiO₂ thin film decorated with Cu₂O nanoparticles by laser ablation », *Opt. Mater.*, vol. 94, p. 130-137, Aug. 2019, DOI: 10.1016/j.optmat.2019.05.030.
- [16] T. T. D. Huynh, A. Petit & N. Semmar, « Picosecond laser induced periodic surface structure on copper thin films », *Appl. Surf. Sci.*, vol. 302, p. 109-113, May 2014, DOI: 10.1016/j.apsusc.2013.10.172.
- [17] A. Talbi *et al.*, « Femtosecond laser irradiation of titanium oxide thin films: accumulation effect under IR beam », *Appl. Phys. A*, vol. 126, n° 5, Art. n° 5, May 2020, DOI: 10.1007/s00339-020-03568-5.
- [18] O. Varlamova, F. Costache, M. Ratzke, & J. Reif, « Control parameters in pattern formation upon femtosecond laser ablation », *Appl. Surf. Sci.*, vol. 253, n° 19, p. 7932-7936, July 2007, DOI: 10.1016/j.apsusc.2007.02.067.
- [19] J. Bonse, A. Rosenfeld, & J. Krüger, « On the role of surface plasmon polaritons in the formation of laser-induced periodic surface structures upon irradiation of silicon by femtosecond-laser pulses », *J. Appl. Phys.*, vol. 106, n° 10, Art. n° 10, Nov. 2009, DOI: 10.1063/1.3261734.
- [20] J. Bonse & J. Krüger, « Pulse number dependence of laser-induced periodic surface structures for femtosecond laser irradiation of silicon », *J. Appl. Phys.*, vol. 108, n° 3, Art. n° 3, Aug. 2010, DOI: 10.1063/1.3456501.
- [21] S. K. Das, H. Messaoudi, A. Debroy, E. McGlynn, & R. Grunwald, « Multiphoton excitation of surface plasmon-polaritons and scaling of nanoripple formation in large bandgap materials », *Opt. Mater. Express*, vol. 3, n° 10, Art. n° 10, Oct. 2013, DOI: 10.1364/OME.3.001705.
- [22] A. Nechache & S. Hody, « Alternative and innovative solid oxide electrolysis cell materials: A short review », *Renew. Sustain. Energy Rev.*, vol. 149, p. 111322, Oct. 2021, DOI: 10.1016/j.rser.2021.111322.
- [23] B. Butz, « Yttria-Doped Zirconia as Solid Electrolyte for Fuel-Cell Applications », Laboratorium für Elektronenmikroskopie (LEM), 2009.
- [24] B. Steele, « Appraisal of Ce_{1-y}Gd_yO_{2-y/2} electrolytes for IT-SOFC operation at 500°C », *Solid State Ion.*, vol. 129, n° 1-4, Art. n° 1-4, Apr. 2000, DOI: 10.1016/S0167-2738(99)00319-7.
- [25] M. Mickan, P. Coddet, J. Vulliet, A. Caillard, T. Sauvage, & A.-L. Thomann, « Optimized magnetron sputtering process for the deposition of gadolinia doped ceria layers with controlled structural properties », *Surf. Coat. Technol.*, vol. 398, p. 126095, Sept. 2020, DOI: 10.1016/j.surfcoat.2020.126095.
- [26] J. Bonse, « Quo Vadis LIPSS?—Recent and Future Trends on Laser-Induced Periodic Surface Structures », *Nanomaterials*, vol. 10, n° 10, p. 1950, Sept. 2020, DOI: 10.3390/nano10101950.
- [27] J. Reif, F. Costache, M. Henyk, & S. V. Pandelov, « Ripples revisited: non-classical morphology at the bottom of femtosecond laser ablation craters in transparent dielectrics », *Appl. Surf. Sci.*, vol. 197-198, p. 891-895, Sept. 2002, DOI: 10.1016/S0169-4332(02)00450-6.
- [28] M. Mezera, J. Bonse, & G. R. B. E. Römer, « Influence of Bulk Temperature on Laser-Induced Periodic Surface Structures on Polycarbonate », *Polymers*, vol. 11, n° 12, p. 1947, Nov. 2019, DOI: 10.3390/polym11121947.
- [29] E. Rebollar, M. Castillejo, & T. A. Ezquerro, « Laser induced periodic surface structures on polymer films: From fundamentals to applications », *Eur. Polym. J.*, vol. 73, p. 162-174, Dec. 2015, DOI: 10.1016/j.eurpolymj.2015.10.012.
- [30] O. Shavdina, H. Rabat, M. Vayer, A. Petit, C. Sinturel, & N. Semmar, « Polystyrene Thin Films Nanostructuring by UV Femtosecond Laser Beam:

- From One Spot to Large Surface », *Nanomaterials*, vol. 11, n° 5, Art. n° 5, Apr. 2021, DOI: 10.3390/nano11051060.
- [31] A. V. Dostovalov *et al.*, « LIPSS on thin metallic films: New insights from multiplicity of laser-excited electromagnetic modes and efficiency of metal oxidation », *Appl. Surf. Sci.*, vol. 491, p. 650-658, Oct. 2019, DOI: 10.1016/j.apsusc.2019.05.171.
- [32] J. Bonse and S. Gräfm « Maxwell Meets Marangoni — A Review of Theories on Laser-Induced Periodic Surface Structures », *Laser Photonics Rev.* 2020, 14, 2000215, DOI: 10.1002/lpor.202000215.
- [33] J. E. Sipe, J. F. Young, J. S. Preston, H. M. van Driel, « Laser-induced periodic surface structure. I. Theory », *Phys. Rev. B*, vol. 27, n° 2, Art. n° 2, Jan. 1983, DOI: 10.1103/PhysRevB.27.1141.
- [34] A. V. Dostovalov, V. P. Korolkov, K. A. Okotrub, K. A. Bronnikov, & S. A. Babin, « Oxide composition and period variation of thermochemical LIPSS on chromium films with different thickness », *Opt. Express*, vol. 26, n° 6, p. 7712, Mar. 2018, DOI: 10.1364/OE.26.007712.
- [35] B. Öktem *et al.*, « Nonlinear laser lithography for indefinitely large-area nanostructuring with femtosecond pulses », *Nat. Photonics*, vol. 7, n° 11, p. 897-901, Nov. 2013, DOI: 10.1038/nphoton.2013.272.
- [36] S. R. Bishop, K. L. Duncan, E. D. Wachsman, « Thermo-Chemical Expansion in Strontium-Doped Lanthanum Cobalt Iron Oxide: Thermo-Chemical Expansion in LSCF », *J. Am. Ceram. Soc.*, vol. 93, n° 12, p. 4115-4121, Dec. 2010, DOI: 10.1111/j.1551-2916.2010.03991.x.
- [37] Y. Kuru, M. Usman, G. Cristiani, & H.-U. Habermeier, « Microstructural changes in epitaxial $\text{YBa}_2\text{Cu}_3\text{O}_{7-\delta}$ thin films due to creation of O vacancies », *J. Cryst. Growth*, vol. 312, n° 20, p. 2904-2908, Oct. 2010, DOI: 10.1016/j.jcrysgro.2010.06.030.
- [38] S. R. Bishop, H. L. Tuller, Y. Kuru, & B. Yildiz, « Chemical expansion of nonstoichiometric $\text{Pr}_{0.1}\text{Ce}_{0.9}\text{O}_{2-\delta}$: Correlation with defect equilibrium model », *J. Eur. Ceram. Soc.*, vol. 31, n° 13, p. 2351-2356, Nov. 2011, DOI: 10.1016/j.jeurceramsoc.2011.05.034.
- [39] Y.-F. Gao *et al.*, « Picosecond laser-induced periodic surface structures (LIPSS) on crystalline silicon », *Surf. Interfaces*, vol. 19, p. 100538, June 2020, DOI: 10.1016/j.surfin.2020.100538.
- [40] J. Bonse, J. Krüger, S. Höhm, & A. Rosenfeld, « Femtosecond laser-induced periodic surface structures », *J. Laser Appl.*, vol. 24, n° 4, Art. n° 4, Sept. 2012, DOI: 10.2351/1.4712658.
- [41] A. Talbi, C. T. Tameko, A. Stolz, E. Millon, C. Boulmer-Leborgne, & N. Semmar, « Nanostructuring of titanium oxide thin film by UV femtosecond laser beam: From one spot to large surfaces », *Appl. Surf. Sci.*, vol. 418, p. 425-429, Oct. 2017, DOI: 10.1016/j.apsusc.2017.02.033.
- [42] M. Ehrhardt, B. Han, F. Frost, P. Lorenz, & K. Zimmer, « Generation of laser-induced periodic surface structures (LIPSS) in fused silica by single NIR nanosecond laser pulse irradiation in confinement », *Appl. Surf. Sci.*, vol. 470, p. 56-62, Mar. 2019, DOI: 10.1016/j.apsusc.2018.11.119.
- [43] L. Parellada-Monreal, I. Castro-Hurtado, M. Martínez-Calderón, L. Presmanes, & G. G. Mandayo, « Laser-induced periodic surface structures on ZnO thin film for high response NO_2 detection », *Appl. Surf. Sci.*, vol. 476, p. 569-575, May 2019, DOI: 10.1016/j.apsusc.2019.01.115.

